Title

Development of a Reactive Force Field for Simulating Photoinitiated Acrylate Polymerization.

Journal

The journal of physical chemistry. B, 127(22)

ISSN

1520-6106

Authors

Huang, Yihan
Karnes, John J
Shusteff, Maxim
et al.

Publication Date

2023-06-01

DOI

10.1021/acs.jpcb.2c09117

Development of a Reactive Force Field for Simulating Photo-initiated Acrylate Polymerization

Yihan Huang[a], John J Karnes[b], Maxim Shusteff[b], Roland Faller[c]*

[a] Department of Materials Science and Engineering, University of California, Davis, CA, USA 95616

[b] Materials Engineering Division, Lawrence Livermore National Laboratory, Livermore, CA, USA 94550

[c] Department of Chemical Engineering, University of California, Davis, CA, USA 95616

* Correspondence: rfaller@ucdavis.edu

KEYWORDS:

Additive manufacturing, ReaxFF parameterization

Abstract

Light-driven and photo-curable polymer based additive manufacturing (AM) has enormous potential due to its excellent resolution and precision. Acrylated radical chain-growth polymerized resins are widely used in photopolymer AM due to their fast kinetics, and often serve as a departure point for developing other resin materials for photopolymer-based AM technologies. For successful control of the photopolymer resins, the molecular basis of the

acrylate free-radical polymerization has to be understood in detail. We present an optimized reactive force field (ReaxFF) for molecular dynamics (MD) simulations of acrylate polymer resins that captures radical polymerization thermodynamics and kinetics. The force field is trained against an extensive training set including density functional theory (DFT) calculations of reaction pathways along the radical polymerization from methyl acrylate to methyl butyrate, bond dissociation energies, and structures and partial charges of several molecules and radicals. We also found that it was critical to train the force field against an incorrect, nonphysical reaction pathway observed in simulations that used parameters not optimized for acrylate polymerization. The parameterization process utilizes a parallelized search algorithm, and the resulting model can describe polymer resin formation, crosslinking density, conversion rate, and residual monomers of the complex acrylate mixtures.

1. Introduction

Photopolymerization-based techniques for additive manufacturing have attracted great interest in the field of biomedical devices, dentistry, tissue engineering, and drug delivery ([1-4])[Quan, 2020 #127], due to their high precision ([5]), mature and commercialized photo-chemical innovations, and environmental and economic benefits ([3-4]). The resins for photopolymerization-based additive manufacturing (AM) consist of photoinitiators and monomers/oligomers in the liquid state. During the AM process, initiating species are generated by light irradiation of the photoinitiators, and they react with monomers/oligomers and then drive the chain growth via radical or cationic reactions ([3]). Because the resins can only be cured under light irradiation, the solid part can be easily separated from the liquid resin after the printing process. Acrylate monomers/oligomers are widely used as photocurable resin materials for commercial products due to their fast kinetics

and compatibility with different form of commercial 3D printers, and they proceed via free-radical polymerization in the AM process (Figure 1). Some of the frequently used acrylates for AM include triethylene glycol diacrylate (TEGDA), 1,6-hexanediol diacrylate (HDDA), pentaerythritol triacrylate (PETA), bisphenol A ethoxylate diacrylate (Bis-EDA), bisphenol A-glycidyl methacrylate (Bis-GMA), and urethane dimethacrylate (UDMA).

Although acrylates demonstrate effectiveness in AM photopolymerization, they still have limitations, and more effort is needed to improve their performance. Acrylate resins tend to shrink during polymerization, and the fast kinetics could result in less uniform networks and hinder the dissipation of shrinkage stress ([3-5]), causing brittleness and cracks. However, both kinetics and shrinkage can be tuned by molecular structure and weight ([3]). Therefore, studies of the acrylate resin materials' design and how it affects the polymerization step and network structure would help improve the mechanical properties of the printed products and create more versatile application scenarios. This work focuses on developing a computational model for acrylate free-radical polymerization that can be used for kinetics and network structure analysis for various acrylate resins.

Quantum chemistry-based methods like density functional theory (DFT) are powerful tools to describe chemical reactions on the atomistic scale. However, this type of calculations is very computationally expensive and thus limits the time scale and length scales. On the other hand, empirical force field methods like classical molecular dynamics (MD) simulation can study the system's dynamic evolution in nanoseconds with thousands of atoms, but loses the reaction information since the atom connectivity is predefined. Therefore, in order to describe the radical chain-growth polymerization kinetics as well as the structural and rheological properties of the acrylate resin, we use ReaxFF-based reactive MD simulation that fills in the gap between

quantum chemistry methods and classical empirical force field methods. ReaxFF is a reactive force field that allows bond formation and dissociation. The total system energy is comprised of bond order (BO) dependent energies that include bond energies (E_{bond}), over-coordination penalties (E_{over}), under-coordination stabilization terms (E_{under}), lone-pair energies (E_{lp}), valence angle energies (E_{val}), and torsion energies ($E_{torsion}$), and non-bonded energies including Coulomb ($E_{coulomb}$) and van der Waals energies ($E_{vdWaals}$) ([6-8]). Bond order is a smooth function of interatomic distance, and the BO dependent energies are functions of BO. Coulomb energy is determined using a geometry-dependent charge distribution scheme, the electronegativity equalization method (EEM), and van der Waals energies account for short-range Pauli repulsion and long-range dispersion ([6, 8]).

The first iteration of the ReaxFF force field was developed by van Duin et al. in 2001 ([6]) for a hydrocarbon system. This was then improved for hydrocarbon combustion by Chenoweth, van Duin, and Goddard in 2008 ([7]). The 2008-C/H/O force field contains H, O, and C, the key elements in acrylate photopolymers. A later revision of the ReaxFF force field, Ti/N/F/C/O/H ([9]) was developed from the 2008-C/H/O force field and parameterized for more elements. However, our MD simulations of acrylate photopolymerization using either the 2008-C/H/O or the Ti/N/F/C/O/H force field resulted in reaction between the radical and the ketone or ether group instead of the reaction between the radical and the vinyl group in the liquid monomer (Figure 2). In order to address this, we utilized the Ti/N/F/C/O/H force field as the starting parameter set and re-optimized the C/O/H parameters to better describe acrylate free-radical polymerization. We retained the parameters of other elements such as Ti, N, and F, as they do not participate in the reactions. Our results highlight the importance of careful selection and optimization of force fields for simulating complex reactive systems.

2. Computational Methods

2.1 Training Set Generation

The optimization process consists of two parts: 1) training set generation and 2) parameterization using the parallel search algorithm.([10]) Force field parameters are determined by minimizing the penalty function (total weighted error):

$$P = \sum_{i}^{train\ set} \left(\frac{V_{i,train} - V_{i,reax}}{\omega_i V_{i,train}} \right)^2 \quad (1)$$

where $V_{i,train}$ is the property value (e.g. energy) from the training set, $V_{i,reax}$ is the property value computed from ReaxFF parameters, and ω_i is the inverse weight that attributes the level of importance of each value during parameterization.

The property values in the training set were all calculated from DFT using the computational chemistry software package Gaussian 16 ([11]). In order to reduce computational expense and increase the transferability among different acrylates, we used the simplest radical reaction where CH_3 radical reacts with the vinyl group in methyl acrylate to produce a methyl butyrate radical as training reaction (Figure 3a). Energies of configurations along the reaction pathway were calculated and the energy differences between the transition state and other configurations, and between the product and reactant were stored in the training set as reaction energies. The energies along the reaction pathway of the unphysical reaction where the radical reacts with the ketone group in methyl acrylate (Figure 3b) were also included because we had to train the force field against the wrong reaction to prevent it from competing with the correct reaction. The radical reacting with the ether group was due to an unphysically weak C-O bond; it cannot happen if the C-O bond orders and bond strengths are correct, so this reaction was not included in the training set. To compare the calculations obtained from the trained ReaxFF force fields to

DFT results, C-C, C=C bonds at the active sites for both methyl acrylate and methyl butyrate were scanned from very short distances to equilibrium distances and then to very large distances without relaxing the whole structure, and the potential energies along the scans were obtained. Calculations were also performed for C-O and C=O bonds in methyl acrylate and methyl butyrate since those bonds behave poorly in the non-optimized force field. The C-H bond was included to ensure that improving the C-C/C=C/C-O/C=O bonds didn't worsen the already good C-H bond. Because the spin multiplicity could change when the bonds were pulled to dissociation and ReaxFF does not treat spin multiplicity explicitly, both singlet and triplet state scans were performed for bonds in methyl acrylate, and doublet and quartet state scans were performed for bonds in methyl butyrate in DFT calculations, and the lower energy points of the two states for each scan were included in the training set as bond dissociation energies to train the ReaxFF parameters. Bond lengths, angles, and atomic partial charges of $CH_3^{\cdot}$, methyl acrylate, methyl butyrate, and the transition state were also included in the training set. Other types of information, for example liquid state density, can also be included in the training set. But in this work, we decided to exclude these and use them as validation after the parameterization, to avoid overfitting. The hybrid Becke, 3-parameter, Lee–Yang–Parr functional B3LYP ([12-13]) and 6311++g(d,p) basis set ([14-15]) were used for all geometry optimizations and energy calculations. The B3LYP functional is sufficient for the development of this force field since its accuracy is beyond what is expected for optimal ReaxFF performance. Consistent with previously developed charge equilibrium protocols for ReaxFF ([6]), we employed Mulliken charge calculation population analysis ([16]) using B3LYP/631g(d,p) ([17]) to calculate DFT partial charges. Although Mulliken is not ideal for fitting dipole and higher charge

moments, it is well-suited for fitting the electronegativity and hardness parameters in the EEM schemes used by ReaxFF([7]).

2.2 Parallel Parameterization Scheme

All ReaxFF parameterization algorithms explore the parameter space and determine the optimum parameters that minimize the penalty function in a similar form as equation 1. Initially, ReaxFF parameterizations were performed using the single-parameter parabolic-search algorithm ([6, 10]) that optimize the force field parameters one at a time by a parabolic extrapolation procedure. This is inefficient and requires significant manual intervention and intuition to determine which set of parameters to optimize first in order to speed up the process. Recent parameterization algorithms include Monte Carlo Simulated Annealing ([18])[Cook, 2020 #144] and Genetic Algorithms ([19]). These algorithms enhance the exploration of the parameter space and allow global optimization, but the number of parameters should be as small as possible to make the procedure feasible ([10, 20]). A typical ReaxFF force field includes hundreds of parameters, and most of them are coupled, so choosing the smallest possible parameter set and determining which parameters to optimize first is difficult. Therefore, we use the parallelized search algorithm ([10]) developed by Deetz et al, to optimize our force field. This algorithm utilizes parallel computing where each processor is assigned a small list of parameters, each parameter is independently evaluated, and all parameters are updated simultaneously after each iteration. Therefore, faster parameterization can be achieved ([10]), and the likelihood of being trapped in local minima is reduced. Not all parameters in the ReaxFF force field need to be optimized. Some of them are not directly related to the reactions of interest, and some are insensitive to the parameterization. Table 1 shows which parameters are chosen and why. The optimization

process is similar to the one in our previous work ([21]), and is described in Supporting Information.

2.3 MD Simulations

All MD simulations were performed in LAMMPS ([22-23]), and all initial configurations with different monomers were independently generated using Packmol ([24]) where molecules are randomly distributed, and atom overlaps were minimized. The initial box sizes were determined assuming the densities of the liquid monomers were the same as experimental values. All initial configurations were subjected to equilibration. During equilibration, a series of short trajectories with short time steps were performed and temperature was carefully ramped up from 100 K to 300 K in NVT (canonical) ensemble followed by 500 ps run in the NPT (isothermal-isobaric) ensemble at 300 K and 1 atm to eliminate any high-energy configurations and relax the systems across the periodic boundaries. The liquid monomer properties were then taken from the equilibrated systems at ambient conditions. For radical polymerization reactions, CH_4 was first introduced to the monomers and once the systems were equilibrated, one of the hydrogens on CH_4 was removed to generate the $CH_3\cdot$ radical and initiate the reaction. Reactions were run in NPT for 20 ns. For all MD simulations, temperature was maintained using a Nosé-Hoover thermostat ([25-26]) with a damping parameter of 25 fs, and pressure was maintained using a Nosé-Hoover barostat with a damping parameter of 250 fs. Except during the temperature ramping process, time steps of 0.25 fs were used for all runs.

3. Results and Discussion

3.1 Force Field Development

The optimized force field, ff.C/H/O/N, agrees well with the DFT partial charges, geometries (bonds and angles), bond dissociation energies, and reaction energies. The differences between

DFT calculated and ReaxFF-fitted average bond lengths and angles were less than 6%, and 3% respectively (Figure 4) showing that the ff.C/H/O/N force field reproduces charge and geometry well for the $CH_3^{\cdot}$, methyl acrylate, methyl butyrate, and the corresponding transition states.

Bond dissociation energy (BDE) scans in Figure 5 and energies along reaction pathways (Figure 6) also show good agreement between DFT and ReaxFF. Including the energetics of the reaction which is not happening in chemical reality into the training process worsens the BDE of the C-O and C=O bonds, and vice versa. So, we penalized this nonphysical reaction such that it has a positive reaction energy and a similar barrier as the correct reaction, while still having reasonable C-O and C=O BDEs. The energy barriers calculated from DFT and ReaxFF of the correct reaction were 3.93 kcal/mol and 5.22 kcal/mol, respectively; those of the wrong reaction were 19.38 kcal/mol and 20.74 kcal/mol, respectively. The reaction energies calculated from DFT and ReaxFF of the correct reaction were -29.80 kcal/mol and -41.27 kcal/mol, respectively; those of the wrong reaction were 2.94 kcal/mol and 0.63 kcal/mol, respectively. The energetics results from the 2008-C/H/O force field and the force field before parameterization were also calculated for comparison. Clearly, the newly developed ReaxFF force field shows an improvement over both. While the force field is not yet fully quantitative, the main improvement is its ability to effectively suppress side reactions. All these comparisons show that the optimized ReaxFF force field can be used for acrylate radical polymerization reactions for the resins under study.

3.2 **Liquid Monomers**

Three different liquid acrylate monomers with different shapes, sizes, and numbers of acrylate functional groups were studied using ff.C/H/O/N. Methyl acrylate (Figure 7a) is a short acrylate

monomer with only one vinyl group, triethylene glycol diacrylate (TEGDA) is a linear acrylate monomer with vinyl groups at each end (Figure 7b), and tris[2-(acryloyloxy)ethyl] isocyanurate (ICN triacrylate) is a three-branched acrylate monomer with a vinyl group at the end of each branch (Figure 7c). Densities were calculated by running MD simulations of the three neat monomer systems with the developed ff.C/H/O/N at 300 K and 1 atm. Three randomly generated initial configurations of each monomer were generated for the average densities. Table 2 shows the ReaxFF calculated densities and the experimentally measured densities, and errors less than 6%. The self-diffusion coefficients *D* were calculated from the mean-square-displacement (MSD) of the monomers:

$$\mathrm{MSD}(t)=\left\langle \left| r(t)-r(0) \right|^2 \right\rangle \tag{2}$$

$$\lim_{t\to\infty} \mathrm{MSD}(t)=¿\,6\,Dt\,¿ \tag{3}$$

which are close to the diffusion coefficients of short linear diacrylate HDDA, long linear diacrylate TEGDA, and branched triacrylate PETA (table 2) calculated using the non-reactive OPLS-AA force field by Karnes et al ([27]). The MSD plot of the three monomers can be found in the Supporting Information. Methyl acrylate is the smallest species among the three and thus diffuses the fastest. ICN-triacrylate is the largest one and it has three branches with three functional groups, and so it diffuses much slower than the two linear monomers.

Radial distribution functions *g(r)* of the vinyl group in the three acrylates and the coordination coord(r) were also calculated from LAMMPS for the three acrylates by equation 4 to investigate the local order:

$$g_{C_{v,A}-C_{v,B}} = \frac{1}{\eta_c}\left\langle \sum_{i=1}^{N} \delta(r - r_i) \right\rangle \quad (4)$$

where C_v is the end carbon in the vinyl group on the reference molecule A or the neighboring molecule B, η_c is a normalization constant to ensure that $g_{1-2}(r \to \infty) = 1$. The coordinations *coord(r)* were calculated by multiplying the integral of *g(r)* by the volume density of the end carbon in the vinyl group (Figure 8). The first maxima of g(r) of all three monomers are around 3.75 Å, and the second maxima of g(r) around 7.25 Å, indicating two solvation shells. The peak heights of the first solvation shells are in the range from 1.3 – 1.5, smaller than highly polar molecular liquids like water, which is about 2.8 ([28]), meaning the local intramolecular order of the acrylates with different shapes and sizes is less than in highly polar liquids. The respective coordination number of vinyl group in the methyl acrylate, TEGDA, and ICN-triacrylate in the first solvation shell was 4.1, 3.4, and 2.1. The diffusive transport and steric access to the reactive site of methyl acrylate are greater than the other two types of acrylate, and so faster free-radical polymerization was expected for the methyl acrylate resin.

3.3 Free-radical Reactions

CH_3 radicals were introduced to the monomer resin to start polymerization, for every 40 monomers there was one radical. 3 CH_4 were randomly distributed within a 26 Å × 26 Å × 26 Å box of 120 methyl acrylates. The periodic simulation box size was chosen to be greater than 2 times of the non-bonded cutoff radius (10 Å) of the force field, and the small box size could reduce the computation cost. Simulation boxes that were four times larger were used to calculate the radial distribution functions of methyl acrylate, TEGDA, and ICN-triacrylate monomers. Since the radial distribution functions (Figure S4) showed very similar structural results to Figure 8, the small box size is suited for this study. The system of methyl acrylate with of CH_4

was equilibrated at 300 K and 1 atm in NPT ensemble, and then temperature was ramped up to 700 K and equilibrated again in NVT ensemble followed by ramping up pressure from 1 atm to 3000 atm in NPT ensemble. Higher temperature was used to speed up the reaction in limited simulation time, and the high pressure was chosen to prevent the system from evaporation and keep the density at the ambient value. One hydrogen from each CH_4 was deleted to create 3 $CH_3\cdot$ radicals and run the reaction at 700 K and 3000 atm in NPT ensemble for 20 ns. All $CH_3\cdot$ radicals reacted with acrylate monomers and initiated the propagations within the first few hundreds of picoseconds, two of the new radicals reacted with other radicals and terminated propagation soon after. One of the radical from the first propagation kept reacting with its neighboring monomers until the radical from the third propagation formed (Figure 9). The activation energy of the first propagation was determined using the Arrhenius equation with simulations performed in the NVT ensemble for 20 ns at 600 K, 700 K, and 800 K (see Figure S5). The calculated activation energy was found to be approximately 7.81 kcal/mol, which closely matches the value obtained from DFT calculations (7.16 kcal/mol).

MD simulations of the same type were performed for TEGDA and ICN-triacrylate, where 1 $CH_3\cdot$ radical and 40 acrylates were randomly distributed in the 33 Å × 33 Å × 33 Å and 39 Å × 39 Å × 39 Å simulation boxes respectively, and ran at 700 K and 3000 atm in the NPT ensemble. This kept the same $CH_3\cdot$ radical concentration as the methyl acrylate system while reducing the computational cost. Due to the differences in shape, size, diffusive transport, and steric access to the reactive site, the TEGDA and ICN-triacrylate systems were expected to propagate slower than methyl acrylate. In 20 ns, the radical initiated the reaction for both TEGDA and ICN-triacrylate systems, and the first propagation for both systems was seen (Figure 10). Further propagations require longer simulation time, but since the local chemistry is the

same as the first propagation, the model developed is expected to be capable of describing full polymerization given additional computer power and simulation time.

4. Conclusion

The optimized ReaxFF force field, ff.C/H/O/N, reproduces the atomic partial charges, geometries, and bond energies of the target acrylates well. More importantly, the reaction energy and barrier calculated from ReaxFF show that the optimized force field can accurately describe the thermodynamics and kinetics of free radical polymerization reaction of the acrylates, and it can be extended to other acrylates like TEGDA and ICN-triacrylate, with correct ReaxFF predicted densities and diffusion coefficients. It can also analyze the diffusive transport and steric access to the functional group and reactive site of different acrylates. Additionally, the thermodynamics and kinetics of the nonphysical radical-keytone reaction, observed during our reparameterization of the 2008-C/H/O force field, had to be included in the training process and the parameters were trained against this unwanted reaction to prevent competition with the correct reactions. Very few works in this field have addressed this issue and optimized the parameter set *against* a reaction in ReaxFF development ([29]). Our results imply that this approach of combining optimization for correct reactions with optimization against incorrect ones will be important going forward for studying increasingly complex chemical systems, with more elements and more possible reaction pathways. The new force field correctly describes the initiation and the following propagations of the radical reacting with liquid acrylate monomers of different size, shape, and number of functional groups. This enables structural, mechanical, thermodynamic, and kinetic analyses of the evolving polymer network during and after cure and will assist in material selection and design of the photoinitiated resins for additive manufacturing

techniques including VAM. Future work will focus on simulations for longer time and comparing the network structure and mechanical properties after curing among various acrylates.

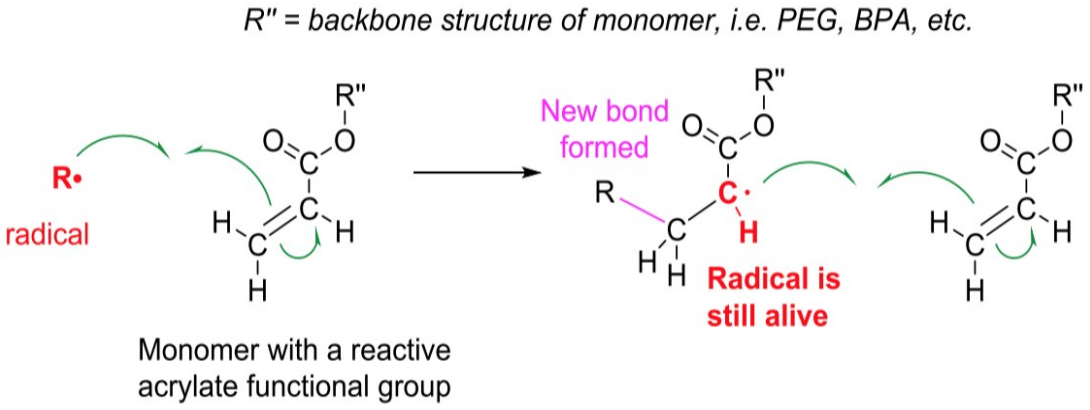

Figure 1. Generalized acrylate free-radical reaction, representing the initiation and propagation steps of a radical-mediated polymerization process. The termination step is not included in this work.

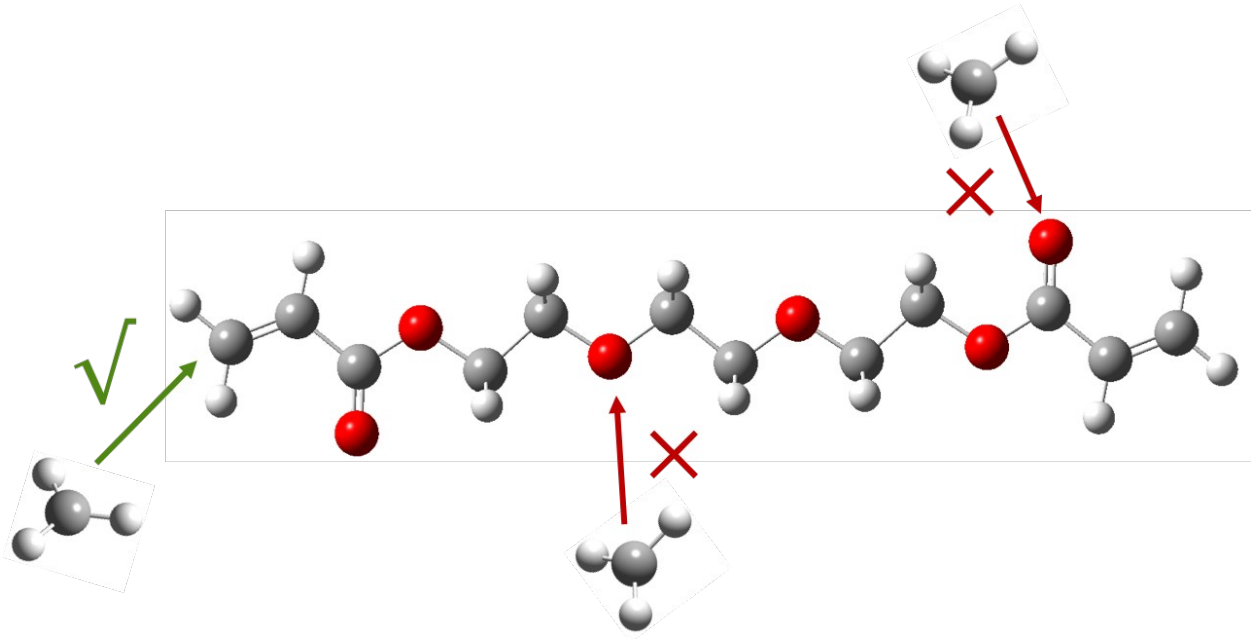

Figure 2. Correct and wrong reaction sites as shown in triethylene glycol diacrylate (TEGDA). Green arrow denotes the correct reaction site, whereas red arrows denotes the wrong reaction sites.

(a) Correct reaction pathway

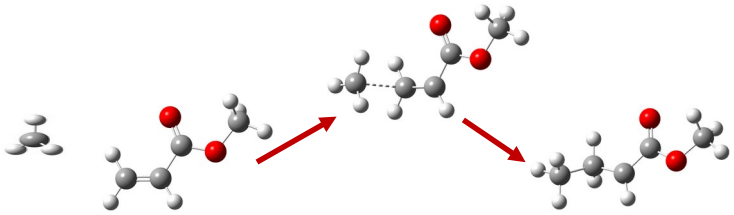

(b) Wrong reaction pathway

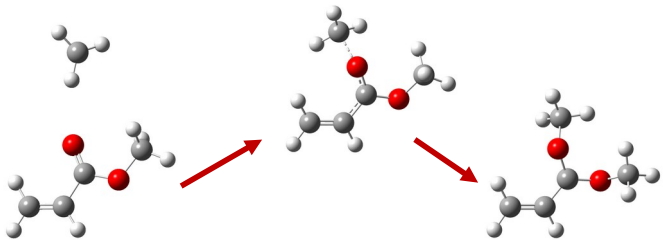

Figure 3. (a) Methyl radical reacts with the vinyl group in methyl acrylate to create the methyl butyrate radical; (b) Methyl radical reacts with the ketone group in methyl acrylate (wrong reaction).

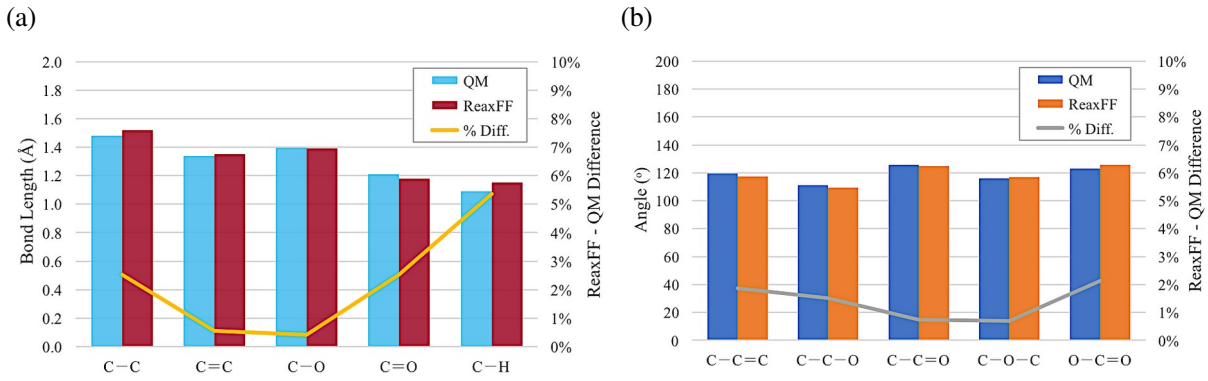

Figure 4. (a) Average bond length differences; (b) Average angle differences.

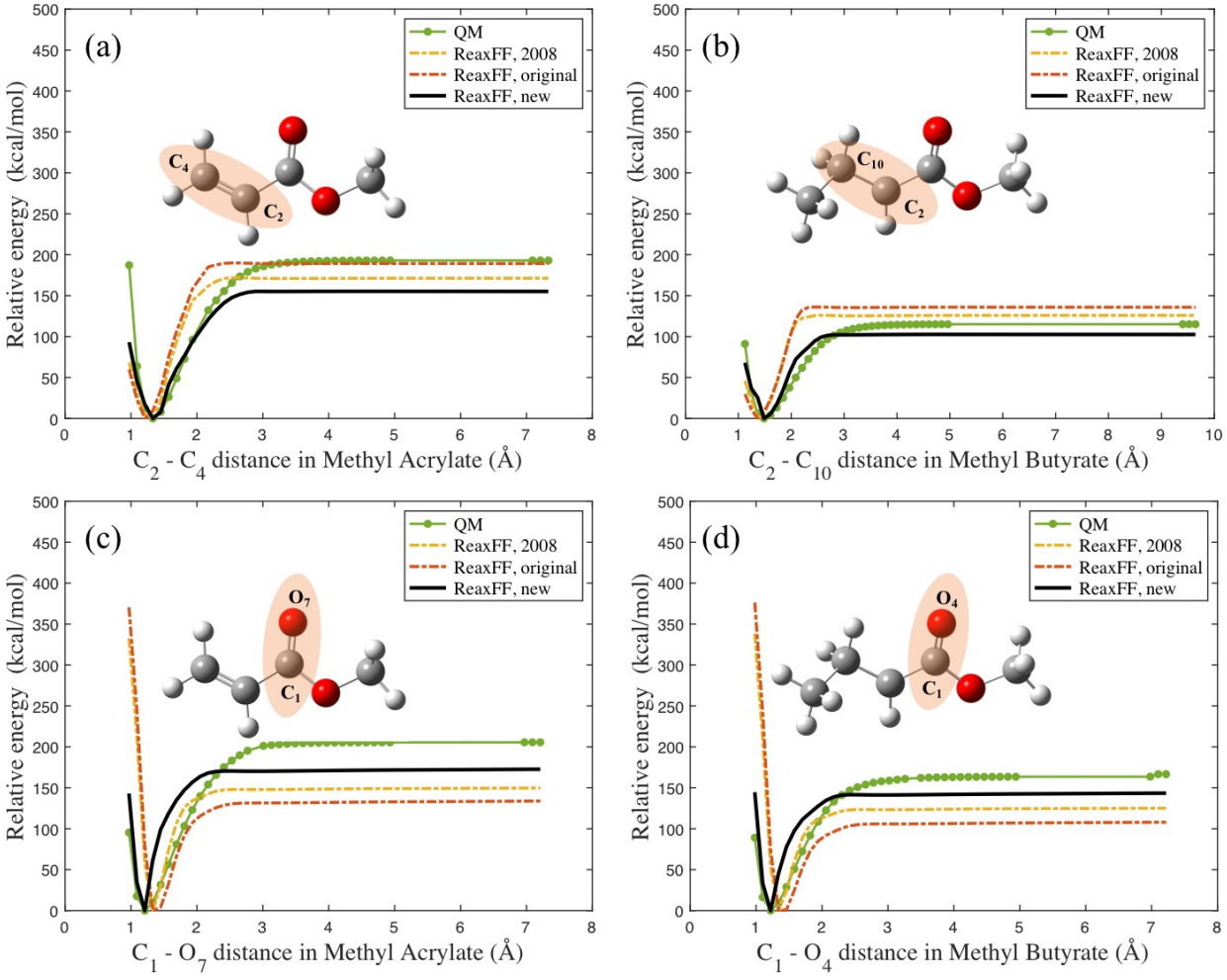

Figure 5. (a-d) Bond dissociation energy scans comparison between quantum mechanical (QM) method (DFT) and ReaxFF, "ReaxFF, new" is the developed force field, "ReaxFF, 2008" is the 2008-C/H/O force field, and "ReaxFF, original" is the force field before parameterization.

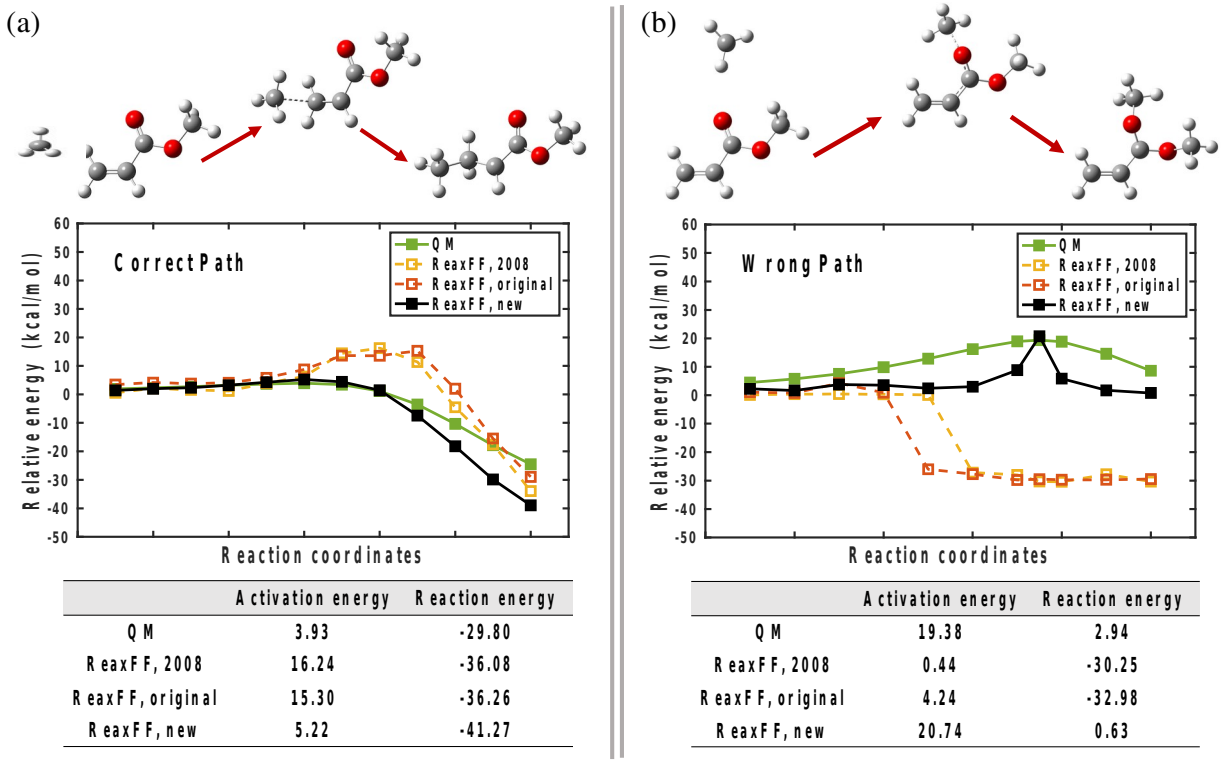

	Activation energy	Reaction energy
QM	3.93	-29.80
ReaxFF, 2008	16.24	-36.08
ReaxFF, original	15.30	-36.26
ReaxFF, new	5.22	-41.27

	Activation energy	Reaction energy
QM	19.38	2.94
ReaxFF, 2008	0.44	-30.25
ReaxFF, original	4.24	-32.98
ReaxFF, new	20.74	0.63

Figure 6. Intrinsic reaction coordinate from quamtum mechanical (QM) method (DFT) vs ReaxFF with barrier and reaction energies. (a) Energies along the correct reaction path; (b) Energies along the wrong reaction path.

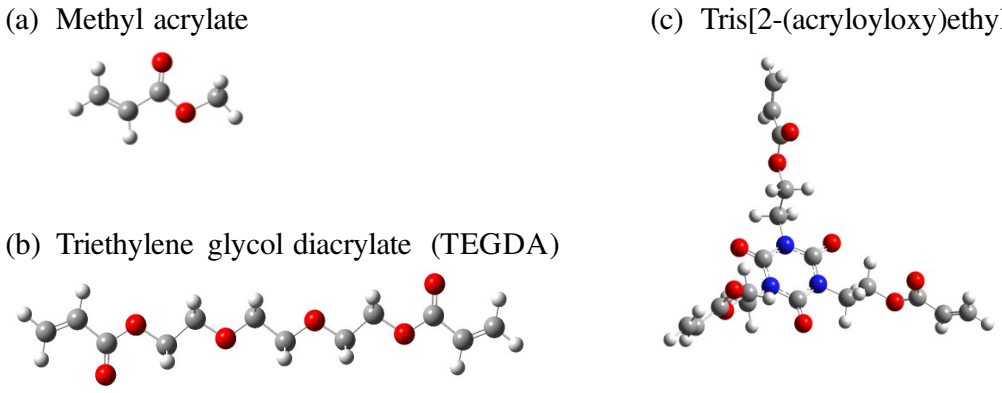

Figure 7. Chemical formulas and representations of (a) methyl acrylate, (b) TEGDA, and (c) ICN triacrylate.

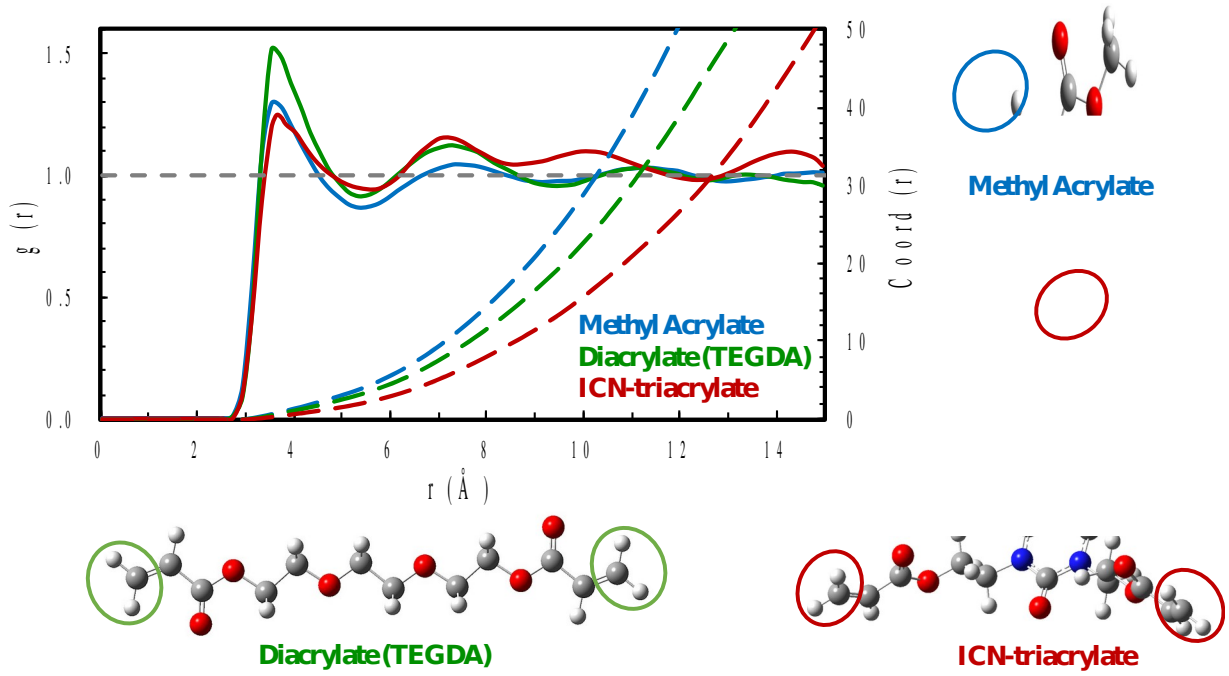

Figure 8. RDF of the vinyl group in acrylates. Solid lines are *g(r)* of the three monomers, and dashed lines are *Coord(r)* of the three monomers. The end carbons in the vinyl groups are circled for each monomer.

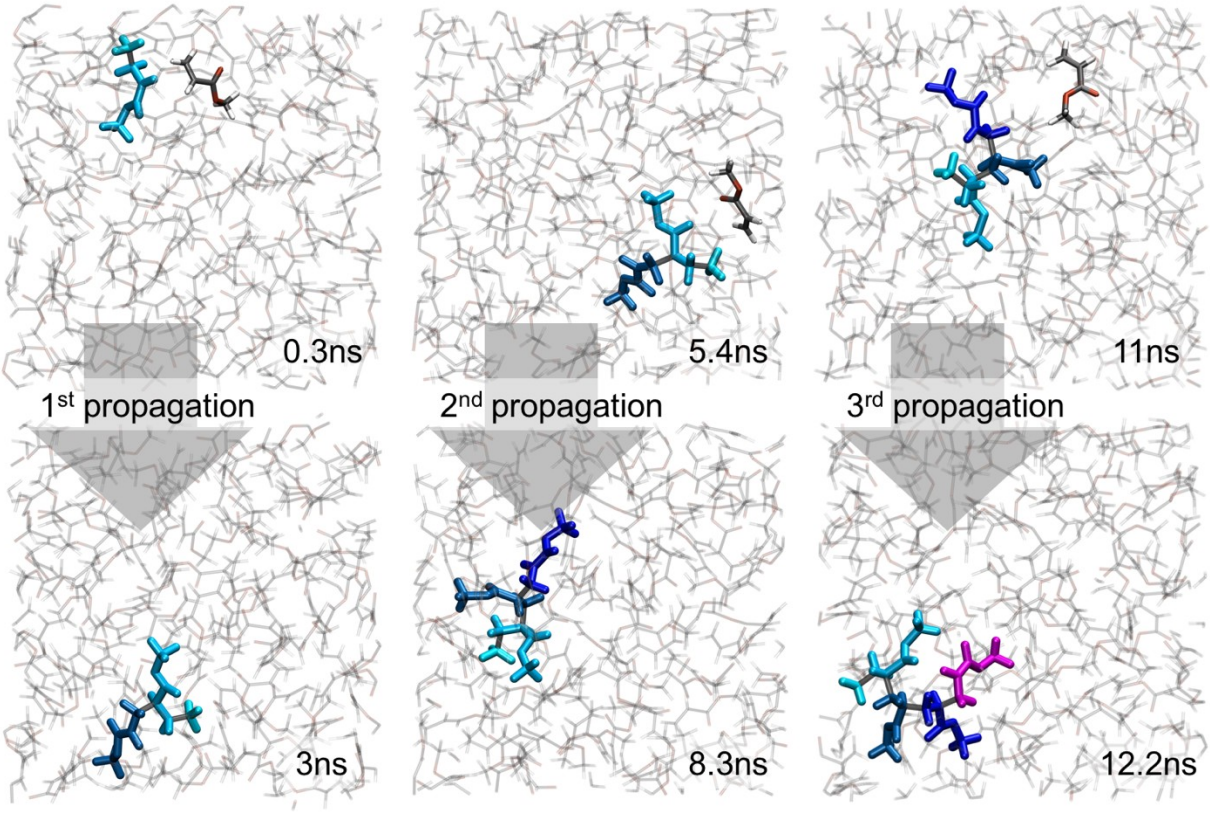

Figure 9. Snapshots of the free-radical polymerization started with methyl acrylate reacting with $CH_3\cdot$ radical. The reacting monomers and $CH_3\cdot$ radical that propagated until the third propagation were shown in colors.

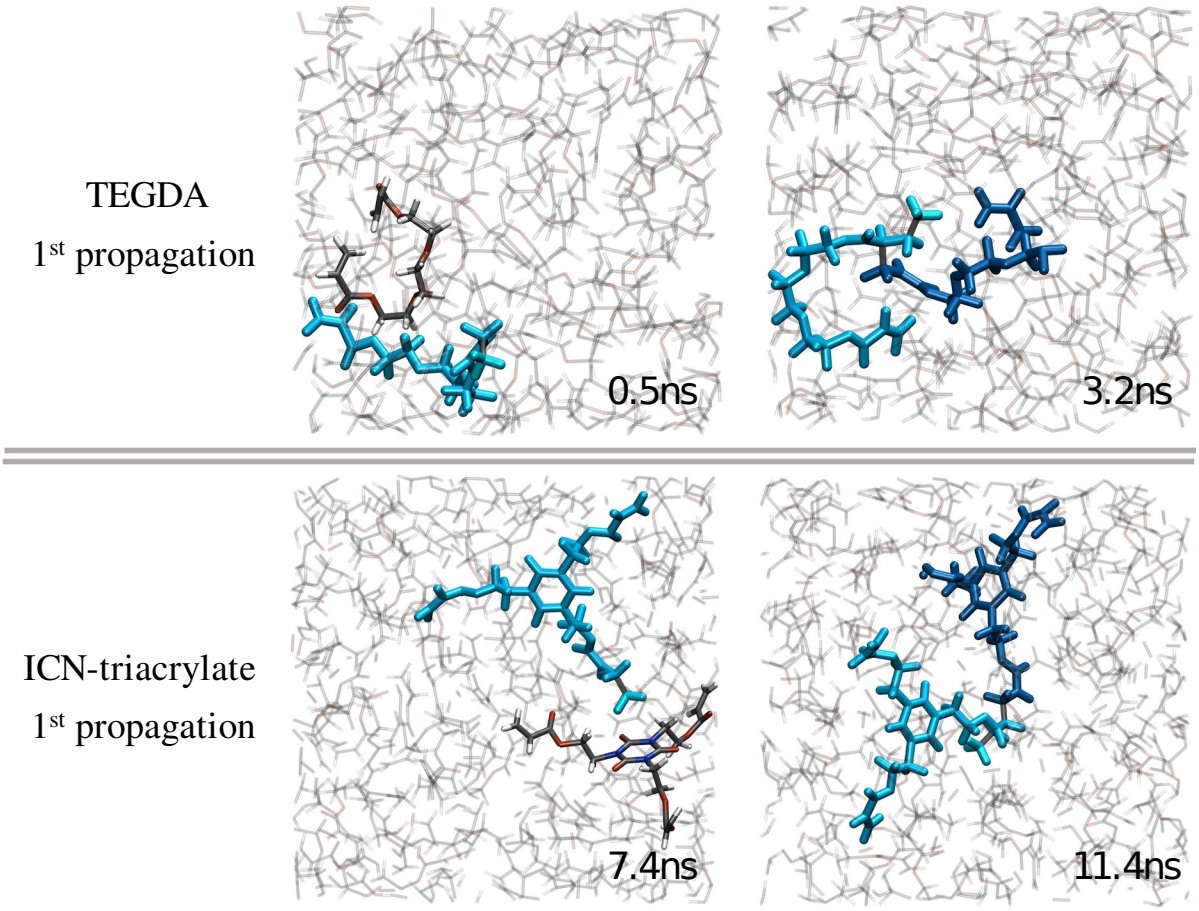

Figure 10. Snapshots of the free-radical polymerization started with $CH_3\cdot$ radical reacting with TEGDA A(top) and ICN-triacrylate (bottom). The reacting monomers and the $CH_3\cdot$ radical are shown in colors.

	Parameters chosen	Reasons for chosen
Electrostatic	Electronegativity equalization method (EEM) parameters for C,H,O	Bonding prediction
Valence bond	All bond radii/order/dissociation energy, and under/over coordination energy parameters for C, H, O atoms and C-C, C-O, C-H pairs	Bonding prediction Reaction pathway Molecular structure
Valence angle	All angle parameters for C, H, O related angles in the molecules	Geometry prediction
Van der Waals	Vdw radii/dissociation energy/shielding for C, H, O	Bonding prediction

Table 1. Choice of force field parameters.

	Density $_{ReaxFF}$ (g/cc)	Density $_{Expt.}$ (g/cc)	Error of Density	D $_{ReaxFF}$ (cm^2/s)
Methyl acrylate	0.99±0.02	0.96	3.13%	4.15×10^{-6}
TEGDA	1.11±0.01	1.12	0.89%	2.67×10^{-7}
ICN-triacrylate	1.23±0.02	1.30	5.33%	6.88×10^{-8}

Table 2. Densities and Diffusion coefficients of methyl acrylate, TEGDA, and ICN-triacrylate.

ASSOCIATED CONTENT

Supporting Information.

The following files are available free of charge.

Supporting Data and Additional Training Results:

This file describes in detail the development and training of the forcefield, particular data:

Figure S1: Workflow of the whole optimization process.

Figure S2: Bond dissociation energies of additional bonds.

Figure S3: MSD plot of three monomers.

Figure S4: RDF of the vinyl group in acrylates, using simulation boxes four times larger than the ones used in Figure 8 of the main text and radical reactions.

Figure S5: Arrhenius plot of the first propagation reaction of the methyl acrylate polymerization, for temperatures at 600 K, 700 K, and 800 K.

ffield.reax.C/H/O/N Final force field for acrylates photopolymerization, can be directly used with the Lammps software

AUTHOR INFORMATION

Corresponding Author

* Correspondence: rfaller@ucdavis.edu

Author Contributions

Yihan Huang performed all the calculations, analysis, and writing of this manuscript; John J. Karnes gave advice on simulations and helped with editing the manuscript; Maxim Shusteff proposed the idea, initiated this project, and helped with editing the manuscript; Roland Faller gave advice on simulations and analysis, helped with editing the manuscript, proposed the idea, and initiated this project. All authors have given approval to the final version of the manuscript.

ACKNOWLEDGMENT

Funding Sources

This work was partially supported by Lawrence Livermore National Laboratory's Laboratory-Directed Research and Development (LDRD) funding and partially performed under the auspices of the U.S. Department of Energy by Lawrence Livermore National Laboratory under Contract DE-AC52-07NA27344, release number LLNL-JRNL-843326.

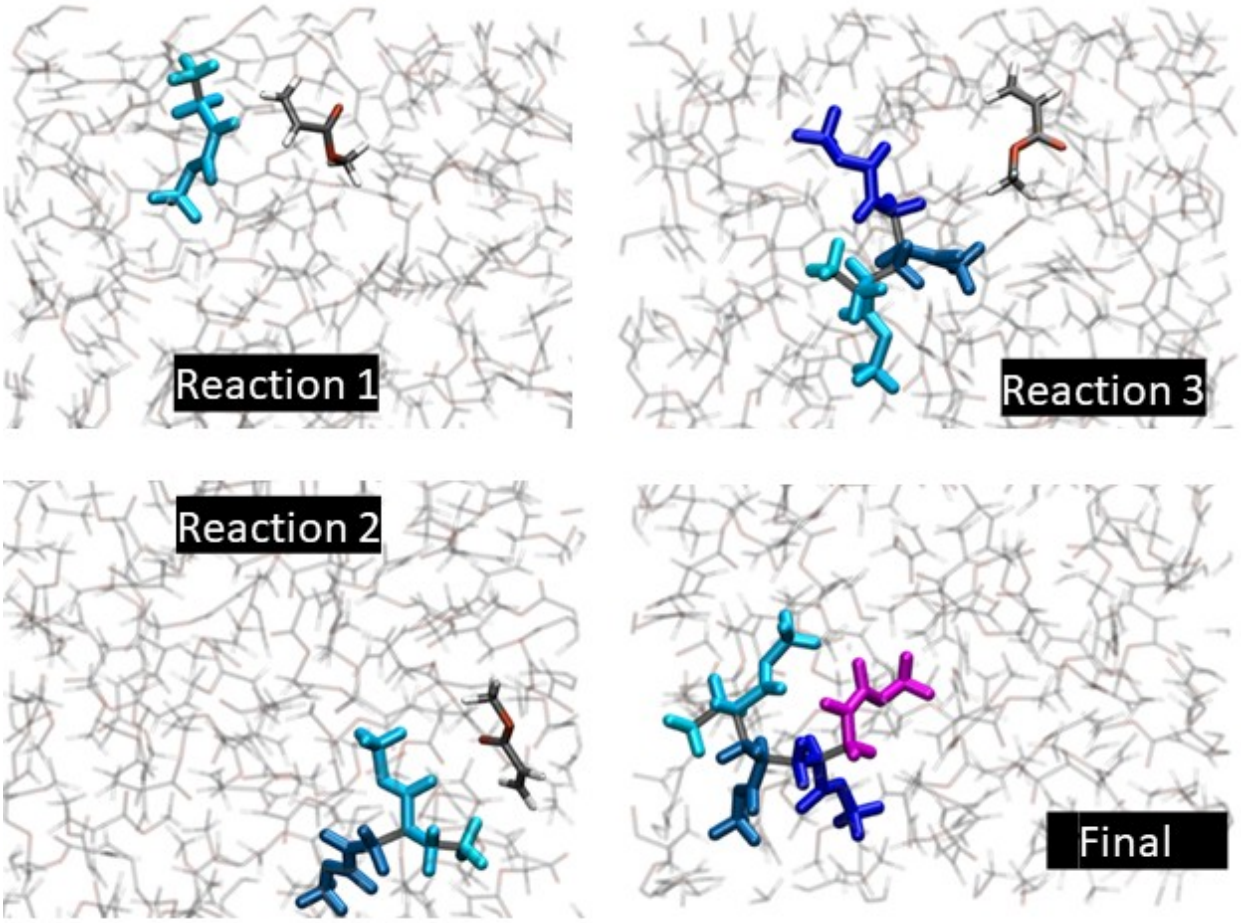

TOC graphic

REFERENCES

1. Wang, M. O.; Vorwald, C. E.; Dreher, M. L.; Mott, E. J.; Cheng, M. H.; Cinar, A.; Mehdizadeh, H.; Somo, S.; Dean, D.; Brey, E. M., Evaluating 3D-Printed biomaterials as scaffolds for vascularized bone tissue engineering. *Advanced Materials* **2015,** *27* (1), 138-144.
2. Rusling, J. F., Developing microfluidic sensing devices using 3D printing. *ACS sensors* **2018,** *3* (3), 522-526.
3. Zhang, J.; Xiao, P., 3D printing of photopolymers. *Polymer Chemistry* **2018,** *9* (13), 1530-1540.
4. Quan, H.; Zhang, T.; Xu, H.; Luo, S.; Nie, J.; Zhu, X., Photo-curing 3D printing technique and its challenges. *Bioactive materials* **2020,** *5* (1), 110-115.
5. Lee, T.; Guymon, C.; Jönsson, E. S.; Hoyle, C. E., The effect of monomer structure on oxygen inhibition of (meth) acrylates photopolymerization. *Polymer* **2004,** *45* (18), 6155-6162.
6. Van Duin, A. C.; Dasgupta, S.; Lorant, F.; Goddard, W. A., ReaxFF: a reactive force field for hydrocarbons. *The Journal of Physical Chemistry A* **2001,** *105* (41), 9396-9409.
7. Chenoweth, K.; Van Duin, A. C.; Goddard, W. A., ReaxFF reactive force field for molecular dynamics simulations of hydrocarbon oxidation. *The Journal of Physical Chemistry A* **2008,** *112* (5), 1040-1053.
8. Senftle, T. P.; Hong, S.; Islam, M. M.; Kylasa, S. B.; Zheng, Y.; Shin, Y. K.; Junkermeier, C.; Engel-Herbert, R.; Janik, M. J.; Aktulga, H. M., The ReaxFF reactive force-field: development, applications and future directions. *npj Computational Materials* **2016,** *2* (1), 1-14.
9. Kim, S.-Y.; van Duin, A. C., Simulation of titanium metal/titanium dioxide etching with chlorine and hydrogen chloride gases using the ReaxFF reactive force field. *The Journal of Physical Chemistry A* **2013,** *117* (27), 5655-5663.
10. Deetz, J. D.; Faller, R., Parallel optimization of a reactive force field for polycondensation of alkoxysilanes. *The Journal of Physical Chemistry B* **2014,** *118* (37), 10966-10978.
11. Frisch, M.; Trucks, G.; Schlegel, H.; Scuseria, G.; Robb, M.; Cheeseman, J.; Scalmani, G.; Barone, V.; Petersson, G.; Nakatsuji, H., Gaussian 16. Gaussian, Inc. Wallingford, CT: 2016.
12. Becke, A. D., Density-functional exchange-energy approximation with correct asymptotic behavior. *Physical review A* **1988,** *38* (6), 3098.
13. Lee, D.; Wexler, A. S., Atmospheric amines–Part III: Photochemistry and toxicity. *Atmospheric environment* **2013,** *71*, 95-103.
14. McLean, A.; Chandler, G., Contracted Gaussian basis sets for molecular calculations. I. Second row atoms, Z= 11–18. *The Journal of chemical physics* **1980,** *72* (10), 5639-5648.
15. Kriihnan, R.; Binkky, J., R. Sceger and JA Pople. *J. Chem. Phys* **1980,** *72*, 650.
16. Mulliken, R. S., Electronic population analysis on LCAO–MO molecular wave functions. I. *The Journal of Chemical Physics* **1955,** *23* (10), 1833-1840.
17. Petersson, G.; Al-Laham, M. A., A complete basis set model chemistry. II. Open-shell systems and the total energies of the first-row atoms. *The Journal of chemical physics* **1991,** *94* (9), 6081-6090.

18. Iype, E.; Hütter, M.; Jansen, A.; Nedea, S. V.; Rindt, C., Parameterization of a reactive force field using a Monte Carlo algorithm. *Journal of computational chemistry* **2013,** *34* (13), 1143-1154.
19. Larsson, H. R.; Van Duin, A. C.; Hartke, B., Global optimization of parameters in the reactive force field ReaxFF for SiOH. *Journal of computational chemistry* **2013,** *34* (25), 2178-2189.
20. Hubin, P. O.; Jacquemin, D.; Leherte, L.; Vercauteren, D. P., Parameterization of the ReaxFF reactive force field for a proline-catalyzed aldol reaction. *Journal of Computational Chemistry* **2016,** *37* (29), 2564-2572.
21. Huang, Y.; Wexler, A. S.; Bein, K. J.; Faller, R., Development of a ReaxFF Force Field for Aqueous Phosphoenolpyruvate as a Novel Biomimetic Carbon Capture Absorbent. *The Journal of Physical Chemistry C* **2022**.
22. Plimpton, S.; Hendrickson, B. In *Parallel molecular dynamics algorithms for simulation of molecular systems*, ACS Symposium Series, Citeseer: 1995; pp 114-114.
23. Thompson, A. P.; Aktulga, H. M.; Berger, R.; Bolintineanu, D. S.; Brown, W. M.; Crozier, P. S.; in't Veld, P. J.; Kohlmeyer, A.; Moore, S. G.; Nguyen, T. D., LAMMPS-a flexible simulation tool for particle-based materials modeling at the atomic, meso, and continuum scales. *Computer Physics Communications* **2022,** *271*, 108171.
24. Martínez, L.; Andrade, R.; Birgin, E. G.; Martínez, J. M., PACKMOL: A package for building initial configurations for molecular dynamics simulations. *Journal of computational chemistry* **2009,** *30* (13), 2157-2164.
25. Nosé, S., A unified formulation of the constant temperature molecular dynamics methods. *The Journal of chemical physics* **1984,** *81* (1), 511-519.
26. Hoover, W. G., Canonical dynamics: Equilibrium phase-space distributions. *Physical review A* **1985,** *31* (3), 1695.
27. Karnes, J. J.; Weisgraber, T. H.; Oakdale, J. S.; Mettry, M.; Shusteff, M.; Biener, J., On the network topology of cross-linked acrylate photopolymers: a molecular dynamics case study. *The Journal of Physical Chemistry B* **2020,** *124* (41), 9204-9215.
28. Laury, M. L.; Wang, L.-P.; Pande, V. S.; Head-Gordon, T.; Ponder, J. W., Revised parameters for the AMOEBA polarizable atomic multipole water model. *The Journal of Physical Chemistry B* **2015,** *119* (29), 9423-9437.
29. McDonnell, M. T.; Keffer, D. J., Reactive molecular dynamics simulations of an excess proton in polyethylene glycol-water solutions. *Molecular Simulation* **2019,** *45* (4-5), 381-393.